Biomedical Optics EXPRESS

Wide-field medium-repetition-rate multiphoton microscopy reduces photodamage of living cells

C. Macias-Romero,[1] V. Zubkovs,[2] S. Wang,[1] and S. Roke[1,*]

[1]*Laboratory for fundamental BioPhotonics, Institute of Bioengineering/Institute of Materials Science, School of Engineering, and Lausanne Centre for Ultrafast Science, École Polytechnique Fédérale de Lausanne, 1015, Lausanne, Switzerland*
[2]*Laboratory of NanoBiotechnology, Institute of Chemical Sciences and Engineering, École Polytechnique Fédérale de Lausanne, 1015, Lausanne, Switzerland*
[*]*sylvie.roke@epfl.ch*

Abstract: Demands of higher spatial and temporal resolutions in linear and nonlinear imaging keep pushing the limits of optical microscopy. We showed recently that a multiphoton microscope with 200 kHz repetition rate and wide-field illumination has a 2-3 orders of magnitude improved throughput compared to a high repetition rate confocal scanning microscope. Here, we examine the photodamage mechanisms and thresholds in live cell imaging for both systems. We first analyze theoretically the temperature increase in an aqueous solution resulting from illuminating with different repetition rates (keeping the deposited energy and irradiated volume constant). The analysis is complemented with photobleaching experiments of a phenolsulfonphthalein (phenol red) solution. Combining medium repetition rates and wide-field illumination promotes thermal diffusivity, which leads to lower photodamage and allows for higher peak intensities. A three day proliferation assay is also performed on living cells to confirm these results: dwell times can be increased by a factor of $3x10^6$ while still preserving cell proliferation. By comparing the proliferation data with the endogenous two-photon fluorescence decay, we propose to use the percentage of the remaining endogenous two-photon fluorescence after exposure as a simple in-situ viability test. These findings enable the possibility of long-term imaging and reduced photodamage.

OCIS codes: (180.4315) Nonlinear microscopy; (180.1790) Confocal microscopy; (170.1530) Cell analysis; (170.2520) Fluorescence microscopy; (170.3880) Medical and biological imaging; (170.0110) Imaging systems.

References and links

1. K. C. Neuman, E. H. Chadd, G. F. Liou, K. Bergman, and S. M. Block, "Characterization of photodamage to escherichia coli in optical traps," Biophys. J. **77**, 2856–2863 (1999).
2. J. Pawley, *Handbook of Biological Confocal Microscopy* (Springer Science, 2006).
3. B. R. Masters and S. Peter, *Handbook of Biomedical Nonlinear Optical Microscopy* (Oxford University Press, 2008).
4. M. S. AlSalhi, M. Atif, a. a. AlObiadi, and a. S. Aldwayyan, "Photodynamic damage study of hela cell line using ala," Laser Physics **21**, 733–739 (2011).
5. K. König, I. Riemann, P. Fischer, and K. Halbhuber, "Intracellular nanourgery with near infrared femtosecond laser pulses," Cell. Mol. Biol. **45**, 195–201 (1999).

#255388 Received 10 Dec 2015; revised 2 Mar 2016; accepted 11 Mar 2016; published 24 Mar 2016

6. K. König, T. W. Becker, P. Fischer, I. Riemann, and K. J. Halbhuber, "Pulse-length dependence of cellular response to intense near-infrared laser pulses in multiphoton microscopes." Opt. Lett. **24**, 113–115 (1999).
7. K. König, H. Liang, M. W. Berns, and B. J. Tromberg, "Cell damage by near-IR microbeams." Nature **377**, 20–21 (1995).
8. K. König, H. Liang, M. W. Berns, and B. J. Tromberg, "Cell damage in near-infrared multimode optical traps as a result of multiphoton absorption," Opt. Lett. **21**, 1090 (1996).
9. K. König, P. T. So, W. W. Mantulin, and E. Gratton, "Cellular response to near-infrared femtosecond laser pulses in two-photon microscopes." Opt. Lett. **22**, 135–136 (1997).
10. E. E. Hoover and J. A. Squier, "Advances in multiphoton microscopy technology," Nat. Photonics **7**, 93–101 (2013).
11. L.-C. Cheng, C.-Y. Chang, C.-Y. Lin, K.-C. Cho, W.-C. Yen, N.-S. Chang, C. Xu, C. Y. Dong, and S.-J. Chen, "Spatiotemporal focusing-based widefield multiphoton microscopy for fast optical sectioning," Opt. Express **20**, 8939–8948 (2012).
12. C. Macias-Romero, M. E. P. Didier, V. Zubkovs, L. Delannoy, F. Dutto, A. Radenovic, and S. Roke, "Probing rotational and translational diffusion of nanodoublers in living cells on microsecond time scales," Nano Lett. **14**, 2552–2557 (2014).
13. C. Macias-Romero, M. E. P. Didier, P. Jourdain, P. Marquet, P. Magistretti, O. B. Tarun, V. Zubkovs, A. Radenovic, and S. Roke, "High throughput second harmonic imaging for label-free biological applications," Opt. Express **22**, 31102–31112 (2014).
14. A. P. Wojtovich and T. H. Foster, "Optogenetic control of ros production," Redox Biology **2**, 368–376 (2014).
15. M. L. Circu and T. Y. Aw, "Reactive oxygen species, cellular redox systems, and apoptosis," Free Radical Biol. Med. **48**, 749–762 (2010).
16. R. W. Boyd, *Nonlinear Optics* (Academic Press, New York, 1992).
17. P. S. Dittrich and P. Schwille, "Photobleaching and stabilization of. fluorophores used for single-molecule analysis with one- and two-photon excitation," Appl. Phys. B **73**, 829–837 (2001).
18. D. J. Sanders, "Temperature distributions produced by scanning gaussian laser beams," Appl. Opt. **23**, 30–35 (1984).
19. S. Kalies, K. Kuetemeyer, and A. Heisterkamp, "Mechanisms of high-order photobleaching and its relationship to intracellular ablation," Bio. Opt. Express **2**, 805–816 (2011).
20. L. Song, E. J. Hennink, I. T. Young, and H. J. Tanke, "Photobleaching kinetics of fluorescein in quantitative fluorescence microscopy," Biophys. J. **68**, 2588–2600 (1995).
21. A. Vogel, J. Noack, G. Hüttman, and G. Paltauf, "Mechanisms of femtosecond laser nanosurgery of cells and tissues," Appl. Phys. B **81**, 1015–1047 (2005).
22. P. Ball, "Water as an active constituent in cell biology," Chem. Rev. **108**, 74–108 (2008).
23. J. R. Lakowicz, "On spectral relaxation in proteins," Photochem. Photobiol. **72**, 421–437 (2000).
24. R. Le Harzic, I. Riemann, K. König, C. Wllner, C. Donitzky, K. Knig, C. Wllner, and C. Donitzky, "Influence of femtosecond laser pulse irradiation on the viability of cells at 1035, 517, and 345 nm," J. Appl. Phys. **102**, 114701 (2007).
25. A. Hopt and E. Neher, "Highly nonlinear photodamage in two-photon fluorescence microscopy." Biophys. J. **80**, 2029–2036 (2001).
26. R. Galli, O. Uckermann, E. F. Andresen, K. D. Geiger, E. Koch, G. Schackert, G. Steiner, and M. Kirsch, "Intrinsic indicator of photodamage during label-free multiphoton microscopy of cells and tissues," PLoS One **9**, e110295 (2014).
27. V. V. Goehukasyan and A. A. Haikal, *Natural Biomarkers for Cellular Matabolism* (CRC Press, 2014).
28. M. R. Kasimova, J. Grigiene, K. Krab, P. H. Hagedorn, H. Flyvbjerg, P. E. Andersen, and I. M. Moller, "The free nadh concentration is kept constant in plant mitochondria under different metabolic conditions," The Plant Cell **18**, 688–698 (2006).
29. H.-W. Wang, Y.-H. Wei, and H.-W. Guo, "Reduced nicotinamide adenine dinucleotide (nadh) fluorescence for the detection of cell death," Anti-Cancer Agents in Med. Chem. **9** (2009).
30. A. Diaspro, G. Chirico, and M. Collini, "Two-photon fluorescence excitation and related techniques in biological microscopy." Q. Rev. Biophys. **38**, 97–166 (2005).
31. U. K. Tirlapur, K. König, C. Peuckert, R. Krieg, and K.-J. Halbhuber, "Femtosecond near-infrared laser pulses elicit generation of reactive oxygen species in mammalian cells leading to apoptosis-like death," Exp. Cell Res. **263**, 88–97 (2001).

1. Introduction

To image living cells, it is required that the optical interactions that give rise to an image does not induce damage [1–5]. This requirement is of particular concern in multiphoton imaging. In order to obtain a good signal-to-noise ratio in multiphoton imaging, high and potentially lethal intensities are required to produce an image [5–9]. The imaging parameters thus have to be

#255388 Received 10 Dec 2015; revised 2 Mar 2016; accepted 11 Mar 2016; published 24 Mar 2016

carefully chosen to prevent damage [2,3]. The most common approach to minimize damage but still obtain the required intensities is [10] to scan a short-pulsed laser (100 fs) with a low pulse energy (0.1 nJ), a high repetition rate (80 MHz), a tight focus (500 nm diam.), and using short dwell times of 10 - 80 μs per pixel [3]. Recent approaches, which are capable of imaging with higher throughput [11–13], use the same pulse duration but with lower repetition rates (100-200 kHz), wide-field illumination (100 μm diam.), and higher pulse energies (0.1 μJ). Such a drastic change of parameters likely brings about changes in the damage mechanisms and in the parameters related to imaging below the photodamage threshold such as peak intensity, fluence, repetition rate and dwell times.

In femtosecond multiphoton microscopy of living systems, three mutually inclusive damage pathways can be identified: ionization, chemical modifications, and thermal damage. Damage due to ionization is produced when free or freed electrons are accelerated, creating plasma bubbles [3], which expand rapidly and destroy or ablate the cell. Chemical or photodynamic damage occurs when reactive oxygen species (ROS) such as [14] O_2^*-, HO^*, RO_2^* or H_2O_2 are created. ROS may react and alter the molecules in the cell before they can be neutralized [14, 15]. During thermal damage, the stored energy from light absorption is converted into thermal energy, which can denaturalize proteins and lead to carbonization or boiling [3]. Thermal energy can originate from non-radiative decays or be transferred from accelerated electrons. In most imaging applications the chemical and thermal damage thresholds are below the ionization threshold [16].

Here, we consider the effects of these three pathways to optical damage and model photodamage using the heat transport equation, paying particular attention to the effects induced by changing from scanning to wide-field imaging and lowering the repetition rate [13]. We combine this analysis with two-photon fluorescence (2PF) experiments of solutions and endogenous in living cells. Combining a proliferation assay and endogenous 2PF experiments we find that a lower repetition rate and a wide field of view allow for a drastic increase of dwell times. We also propose an in-situ viability test based on the decay of endogenous 2PF signals.

2. Photodamage mechanisms

In general, chemical and thermal damage processes are governed by the mobility of activated molecules and heat diffusion [2, 17, 18]. The effective duration of the applied energy load and the thermal diffusivity are thus key parameters to determine the photodamage threshold in cells. The effective duration has two temporal components: the pulse duration and the time between pulses. Nanosecond pulses increase the temperature in aqueous solutions more than femtosecond pulses that have the same peak intensity. The thermal (or chemical) load induced by a single femtosecond pulse may be negligible, but the accumulative effect of several pulses can easily lead to damage; in this case the time between pulses also needs to be considered. Cell damage caused by denaturalization or ROS production is more likely to occur if energy is delivered to a molecule that is already in an excited state [19]. The typical lifetime of a singlet excited state in fluorophores [20] can be between 1-10 ns, and the time between laser pulses in high repetition rate microscopes (e.g. 88 MHz) is 11 ns. The fluorophore may thus still be in an excited state by the arrival of the next pulse leading to accumulation. The accumulation of energy will then increase the probability of denaturalization, saturation or photobleaching and produce a temperature increase. In contrast, with $\sim$100 kHz repetition rates the time between pulses is 10 μs. The fluorophore will most likely be in a relaxed (ground) state before the next pulse arrives, avoiding accumulation of energy. In this case the time between pulses is closer to thermal diffusivity rates in liquids ($\sim$1 $\mu m^2/\mu s$). Therefore, inter-pulse thermal diffusion can be promoted by appropriately choosing the physical dimension of the energy source (i.e. the illuminating spot). We thus expect that the repetition rate of the illumination source and its

#255388 Received 10 Dec 2015; revised 2 Mar 2016; accepted 11 Mar 2016; published 24 Mar 2016

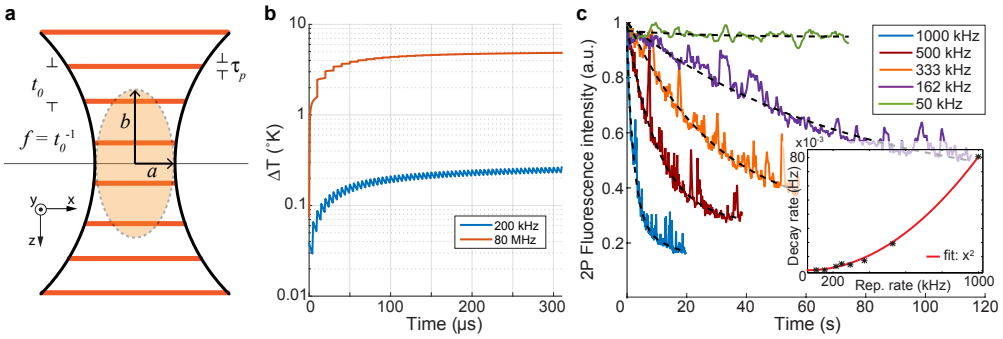

Fig. 1. Simulations of heat flow and photobleaching experiments for different illuminating repetition rates (a) Schematic of a focused pulsed Gaussian beam. (b) Calculated temperature rise in the same volume of water following a 80 MHz (scanning illumination, red), and a wide-field illumination (blue) with the same deposited and absorbed peak intensity (1 J/cm^3). Less heat is accumulated in the water when illuminating with the wide-field and lower repetition rate system. (c) Two-photon fluorescence (2PF) intensity decay due to photobleaching of a solution of phenolsulfonphthalein (phenol red) as a function of time. The solution is illuminated at constant peak intensity (83 GW/cm^2) and cumulative fluence (20x10^6 pulses) using different repetition rates (and hence different powers and recording times). The inset shows the photobleaching decay rates obtained from the 2PF intensity decay as a function of the illumination repetition rate (fitted with a quadratic function). For a constant peak intensity, the photobleaching decay rate depends quadratically on the repetition rate and hence on the power.

size will be key parameters in determining the degree of photodamage in live cell imaging. In what follows, we quantify the optical processes that lead to damage, we use the peak intensity (the ratio of pulse energy over area and pulse duration) in combination with the repetition rate. Both parameters combine to a measure of the temporal and spatial photon density as well as an indication for which process might be relevant for the energy dissipation (i.e. thermal or chemical).

To explore the importance of the repetition rate in photodamage processes we first consider the heat transport equation. With this equation we can calculate the (position dependent) temperature rise (ΔT) in a liquid due to the interaction with a pulsed focused Gaussian beam, see Fig 1(a). The temperature rise can be written as [18, 21]

$$\Delta T(x,y,z,t) = \sum_{n=0}^{\mathrm{int}(t*f)} \int_0^{\tau_p} \frac{A\sqrt{2}}{8\pi^2 C_p \left[\kappa(t-t'-n/f)\right]^{3/2}} \iiint_{-\infty}^{\infty} e^{-\frac{2(x'^2+y'^2)}{a^2} - \frac{2z'^2}{b^2} - \frac{(x-x')^2+(y-y')^2+(z-z')^2}{4\kappa(t-t'-n/f)}} dx'dy'dz'dt'. \quad (1)$$

Here the illumination is characterized by the repetition rate f (Hz), the deposited energy by a single pulse E (J), and the half axes a and b of the transverse and longitudinal dimensions of the heat source (measured as 1/e^2 in m, Fig. 1(a)). The material is characterized by the absorption coefficient α (m^{-1}), the thermal diffusivity κ (m^2/s), the heat capacity C_P (J/K), and the density ρ (kg/m^3). The summation index denoted by n represents the arrival of the n^{th} pulse. The interaction of the laser beam with the material is characterized by the absorbed intensity $A = \alpha' E/(\pi a^2 b)$, where $\alpha' = 2\alpha b$. We can then calculate the temperature rise in water, which is a good zero-order estimation of the minimum temperature increase that can be found in a

#255388 Received 10 Dec 2015; revised 2 Mar 2016; accepted 11 Mar 2016; published 24 Mar 2016

living cell [22] (given that 60% of its contents is water). Figure 1(b) shows the rise in temperature calculated for two cases keeping the illuminated volume and deposited energy constant: First, the effect of tightly focused beam (1.1 NA, 1035 nm wavelength, 80 MHz repetition rate, red curve), exemplary of a point scanning multiphoton microscope is considered. Second the effect of a weakly focused beam (0.02 NA, 1035 nm wavelength, 200 kHz repetition rate, blue curve), exemplary of a wide-field imaging system is computed [13]. For the scanning system, we considered a dwell time of 10 μs and a scanning resolution equal to a. To compare both cases, we used the same absorbed peak intensity (1 J/cm^3) and the same effective illuminated transverse section and volume (20 μm$^2\times$ 5 μm). For the scanning illumination a = 0.443 μm and b = 1.6 μm. For the wide-field illumination a = 5 μm and b = 5 μm. The temperature rise was calculated at the center of the beam (i.e. x,y,z = 0).

Figure 1(b) shows that the temperature rise is an order of magnitude higher for the 80 MHz system compared to the 200 kHz system. The reason is that with a lower repetition rate system the time between pulses is enough to allow for heat dissipation, which is not the case for the high repetition rate system. These simulations show that in addition to the peak intensity, the product of irradiated volume and repetition rate (i.e. $f\pi a^2 b$) is important. Laser damage indicators, such as fluence or peak intensity, do not take this product into account. In order for the wide-field and scanning systems to display the same temperature rise after an illumination time of 5 ms, the imaging volume in the wide-field system would have to be increased by 255 times. With such an increase in the volume and the scanning parameters given above, a 270–fold improvement in the imaging throughput is expected with the wide-field configuration, which is indeed observed ([13], Eq. 2, Fig. 3(a)).

The effect of the illumination repetition rates can be studied experimentally by recording the 2PF intensity decay of a solution containing phenolsulfonphthalein (phenol red) for different illuminating repetition rates. Figure 1(c) shows the 2PF intensity decay over time (due to photobleaching) for an aqueous solution of phenol red solution that is illuminated with pulses that have a constant peak intensity (82 GW/cm^2 or 14 mJ/cm^2 at 170 fs) and cumulative fluence (number of delivered pulses: 20x10^6) but different repetition rates. The traces were fitted with an exponential function, $I(t) = e^{-\sigma t}$, from which the photobleaching decay rate σ is obtained [20, 23]. The inset shows the decay rates obtained as a function of the different illuminating repetition rates. It can be seen that at 50 kHz no photobleaching occurs. Note that the imaging time was 400 s (not fully shown on the graph). Increasing the repetition rate induces a higher 2PF decay rate (i.e. more photobleaching), even though the light in all cases has the same peak intensity and cumulative fluence (i.e. the total amount of generated nonlinear photons is the same in all cases). Clearly, the accumulation and dissipation of energy play a more important role in the photobleaching process than the peak intensity.

3. Proliferation assay on HEK cells

To put these findings into practice and to examine the photodamage-free imaging possibilities using wide-field medium repetition rate illumination, we performed a proliferation assay on human embryonic kidney (HEK) cells. We exposed HEK cells to different peak intensities keeping the illuminating time constant (30 s), and different illuminating times at constant peak intensity. We then tracked their proliferation over 3 days. Figure 2 shows the procedure of the experiment (a), phase contrast images of the control cells after 3 days of the exposure (inset), and histograms of the results of the proliferation assay (b,c). Figure 2(b) shows the proliferation efficiency obtained when the exposure time is kept constant (30 s) and the peak intensity is varied. Figure 2(c) shows the proliferation efficiency obtained for constant intensity (60 GW/cm^2) and varying illuminating time. Figure 2(b) shows that the proliferation remains positive after the cells are irradiated with 43 GW/cm^2 (7.3 mJ/cm^2 @170 fs). The growth is

#255388 Received 10 Dec 2015; revised 2 Mar 2016; accepted 11 Mar 2016; published 24 Mar 2016

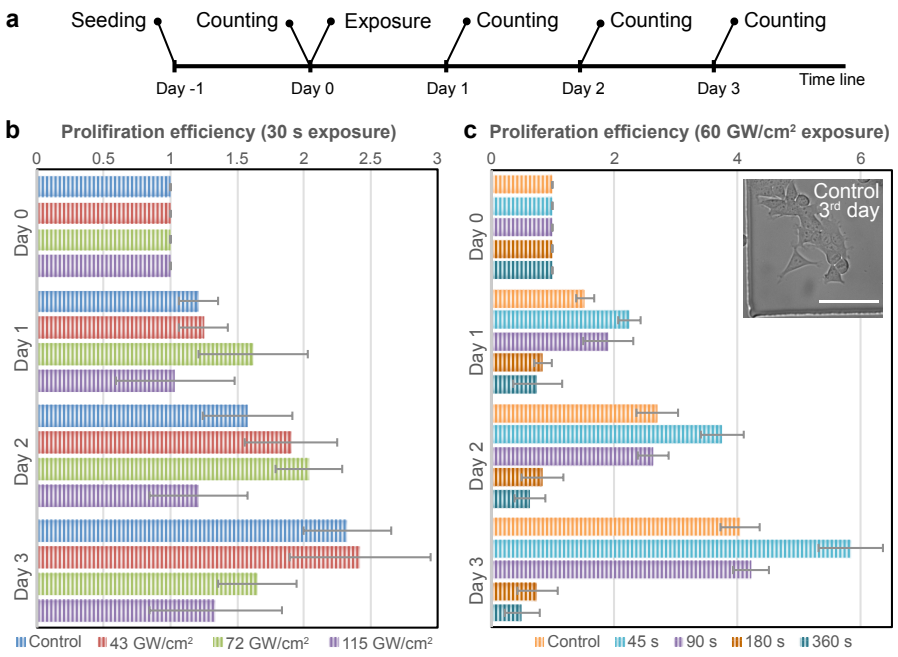

Fig. 2. Proliferation assay of human embryonic kidney (HEK) 293 cells after illumination with 1035 nm, 170 fs, 200 kHz laser pulses with listed peak intensities. (a) Timeline of the experiment. (b) Histogram of the proliferation efficiency on the first, second, and third day after 30 s exposures with different peak intensities. (c) Histogram of the proliferation efficiency for the same peak intensity (60 GW/cm^2) but different exposure times. The inset shows a phase contrast image of the control (unexposed) cells three days after exposure (scale bar: 50 μm). The error bars represent the standard deviation of the cell count.

clearly hampered after irradiation with 115 GW/cm^2 (19.6 mJ/cm^2 @170 fs). A decline is observed only after the 3rd day when irradiated with 72 GW/cm^2 (12.2 mJ/cm^2 @170 fs). This decline may originate from the migration of the cells to neighboring units. Thus, between 43 and 72 GW/cm^2 the cells become agitated but not to the degree that they stop their reproduction cycle or lose their ability to respond to the environment and move. Figure 2(c) shows that exposing the cells to the same peak intensity but during different lengths of time can hinder the cell proliferation. Proliferation is clearly hampered if the cells are exposed to more than 180 s with an illumination of 60 GW/cm^2. Next, we compare these numbers to previously published studies of laser induced cell damage.

Table 1 summarizes the results of Fig. 2 and compares them to previously published viability studies, displaying the dwell time, allowed peak intensities, and throughput factor, which is a measure of the number of photons per area per second that can be generated with the given illumination parameters (see Eq. 2 Ref. [13]); a higher number indicates a better imaging throughput. It can be seen that for a medium repetition rate (100 kHz) and a tight focus (500 nm diameter), very high peak intensities (900 - 2000 GW/cm^2) can be used [24]. This comes, however, at the cost of a very inefficient imaging process. Being able to use such high peak intensities agrees with the results from the photobleaching experiment above and is clear indication that allowing for energy dissipation is very important for cell viability. The likelihood of producing ROS, avalanche breakdown, or simply thermal damage increases if the system is already in an excited state. Consequently, a significant improvement in the illumination (dwell)

#255388 Received 10 Dec 2015; revised 2 Mar 2016; accepted 11 Mar 2016; published 24 Mar 2016

Table 1. Results of different cell viability studies, including the current one, as a function of illuminating peak intensities.

Laser wavelength, nm	Pulse duration, fs	Repetition rate, MHz	Cell line	Method of characterization	Dwell time	Peak intensities GW/cm^2			Throughput ratio	Reference
						Tolerable	Indirect damage	Lethal damage		
517	393	0.1	CHO	Proliferation	50 µs	5604	9805	14012	2x10^{-4}	[24]
800	150	80	CHO	Proliferation	80 µs	20	49	111	.15	[9]
840	190	82	AC	Ca2+ release indicator / Degranulation	10 µs	19	28	52	25	[25]
1035	**170**	**0.2**	**HEK**	**Proliferation / photobleaching**	**30 s**	**43**	**72**	**115**	**100**	**This work**
1035	393	0.1	CHO	Proliferation	50 µs	971	2073	3110	2x10^{-4}	[24]

Abbreviations: CHO: Chinese hamster ovary [24]; AC: Adrenal chromaffin [9]; HEK: human embryo kidney [25].

time can be obtained with a wide-field medium repetition rate approach (i.e. 90 s vs. 10-80 μs).

4. Photobleaching as a viability indicator

The dependence of the damage thresholds on the peak intensity, repetition rate, and thermal diffusivity makes it difficult to find a single figure of merit that determines the damage threshold. Performing standard viability tests for every setting can be very expensive, time consuming, and in some cases not possible (e.g. when performing in-vivo experiments). Therefore, there is a need for simple and inexpensive in-situ viability tests [26].

It has been shown that high concentrations of mitochondrial ROS promotes cell apoptosis [15]. High oxidative stress induces ROS formation in the mitochondria, which leads to mitochondrial permeabilization and the release of factors that induce cell apoptosis. Additionally, the excess of intracellular ROS interacts unfavorably with all the surrounding metabolites before they can be neutralized by the antioxidants in the cell. The affected molecules include fluorescent coenzymes such as flavin adenine dinucleotides (FAD) and nicotinamide adenine dinucleotide (NAD+), which are essential to the cellular metabolism [27–29]. These coenzyme families are responsible for most of the endogenous 2PF in cells [30]. The lack or reduction of endogenous 2PF in the cell thus suggests that the viability of the cell has been compromised. Kalies et al. [19] showed that the photobleaching half-life of exogenous 2PF fluorophores matches the half-saturation value of the ROS production, and Tirlapur et al. [31] showed that the ROS production is increased when illuminating with a fs laser pulse leading to cell apoptosis. These findings indicate that there is a correlation between endogenous 2PF, apoptosis, ROS production, and illuminating intensity. The fs laser produces ROS species that will affect (proportionally) the level of endogenous 2PF and the viability of the cell. We thus propose as a simple in-situ viability test to use the percentage of the remaining endogenous 2PF intensity (in wide-field systems) as a damage indicator.

To investigate the possible correlation between photodamage and reduction of endogenous 2PF, we measured the photobleaching of endogenous 2PF during a proliferation assay, as displayed in Fig. 3(a). The photobleaching data is fitted with an exponential function to obtain a

#255388 Received 10 Dec 2015; revised 2 Mar 2016; accepted 11 Mar 2016; published 24 Mar 2016

series of decay rates for different peak intensities (Fig. 3(b), see Section 6 for more information). With the decay rates, we can then calculate the percentage of endogenous 2PF intensity that would remain after 30 seconds of exposure. Knowing at which peak intensity damage is done (Figure 2, Table 1), we can correlate the percentage of remaining 2PF intensity to the measured damage thresholds, see Fig. 3(c). The zones for no damage (green), possible indirect damage (yellow) and lethal damage (red) are indicated in the graph. Indirect damage is observed when the remaining endogenous 2PF is between 15% and 30%, while irreversible damage is produced when it drops below 30%. Note that the damage may only be linked to the drop of endogenous (and not exogenous) fluorescence. The drop in endogenous 2PF is an indicator that local coenzymes vital to the cell have been compromised; while a drop in exogenous fluorescence may only indicate that the fluorophore has been destroyed without any repercussions to the cell [19].

Further confirmation of the correspondence between the percentage of endogenous 2PF photobleaching and cell damage can be sought by correlating cell proliferation with the intensity decay when the same peak intensity but different exposure time are used, as shown in Fig. 2(c). Figure 3(d) plots the percentage of the endogenous 2PF intensity decay as a function of time (up to 370 s) that results from exposing the cells to 60 GW/cm^2. The red markers denote the exposure times used in the proliferation experiment of Fig. 2(c), i.e. 45 s, 90 s, 180 s, and 360 s. Here too we observe that when illuminating continuously with a constant peak intensity, a decay greater than 30% in the endogenous 2PF intensity corresponds to a hindered cell proliferation.

5. Conclusions

We determined the optical parameters that allow for damage- and label-free imaging of live cells using wide-field medium-repetition-rate multiphoton microscopy. We observed that photobleaching of phenol red is absent when using high peak intensities (82 GW/cm^2), a medium-ranged repetition rate (50-100 kHz) and long exposure (dwell) times (400 s). We performed as well a 3-day proliferation assay on HEK cells to confirm the benefits of wide-field medium-repetition-rate illumination. Proliferation was conserved after exposures of up to 72 GW/cm^2 during 30 s. Proliferation was compromised after 30 s exposure to 115 GW/cm^2. We also observed that proliferation depends on the exposure time when illuminating with a constant peak intensity. Proliferation was conserved after exposure to 60 GW/cm^2 for up to 90 s, but the proliferation was hindered when the exposure time is beyond 180 s, which corresponded to a decay beyond 30% in the endogenous 2PF intensity. Compared to scanning systems, the dwell times used here were increased by a factor of 3×10^6 while still preserving cell proliferation. This improvement can be explained by noting that in a wide-field configuration the probability of thermal and chemical damage is reduced when illuminating with medium repetition rates ($<$200 kHz). To prevent photodamage, allowing for electronic relaxation and promoting thermal diffusivity is as important as using low peak intensities. We also proposed as a simple in-situ viability test to use the percentage of the remaining endogenous 2PF after exposure. Lethal damage is observed in the cells when the endogenous 2PF is reduced by more than 30%.

6. Materials and methods

Cell culture. Human embryonic kidney 293 cells (ATCC CRL-1573) were purchased from ATCC biological resource center (LGC Standards, Molsheim, France). The cells were cultured in Dulbecco's modified Eagle's medium (DMEM) (Gibco, Live Technologies) with 4.5 g/L glucose, L-glutamine, 10% fetal calf serum and 1% of 100 units/ml penicillin / 100 mg/ml streptomycin at 37°C in a humidified, 5% CO_2 incubator (Gibco, Live Technologies). We recultured the cells on gridded cell culture dishes (IBIDI, μ-Dish Grid-500), which were precoated with poly-L-lysine (0.3% in buffer solution, Sigma Aldrich) for 30 min at 37°C. We

#255388 Received 10 Dec 2015; revised 2 Mar 2016; accepted 11 Mar 2016; published 24 Mar 2016

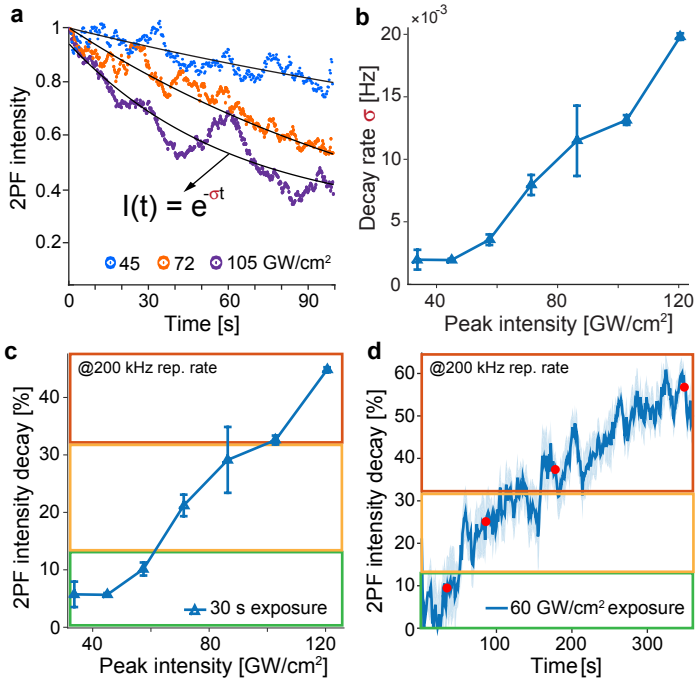

Fig. 3. (a) Examples of the endogenous 2PF intensity decays in the HEK cells for different illuminating peak intensities. (b) Decay rates obtained from fitting the intensity decay of the endogenous 2PF with an exponential function. (c) Percentage of 2PF intensity lost after 30 s of exposure with the different peak intensities. (d) Percentage of 2PF intensity lost over time when exposing the cells during 370 s to 60 GW/cm^2. The red markers represent the exposure times used in the proliferation experiment shown in Fig. 2(c). The error bars and shaded area in (d) represent the standard deviation from 20-30 measurements.

incubated the cells for 24 h (allowing the healthy cells attach to the bottom on the dish) and exchanged the cell culture media 30 min before the exposure experiment.

Optical setup. The optical setup has been described in detail elsewhere [13]. The repetition rate was varied by changing the configuration of the pulse picker via software (Pharos, Light-Conversion). We could thus ensure that the pulses had the same energy, shape in time, and duration independently of the repetition rate. To measure 2PF, a short- (900 nm, Thorlabs) and a long-pass filter (550 nm, Thorlabs) were placed before the camera.

Proliferation assay. Within the same gridded dish, three sections were selected at random as control and three other sections were selected for the exposure experiments. All the cells within the three selected experiment sections were exposed to same peak intensity and time. One experiment consisted on exposing the cells for 30 seconds and varying peak intensities. Another experiment consisted of exposing the cells to the same peak intensity but different times. Each section was exposed for n seconds, and different dishes were used for different peak intensities. The dish was closed during the three days following exposure. The number of exposed cells on Day 0 was between 10 and 170 cells per section. The cells were maintained in incubator conditions for the following days. We recorded visible light phase contrast images of the exposed and control sections before exposure and 24 h, 48 h, and 72 h after exposure. We counted the number of the cells in the images of each section using the ImageJ Cell Counter plug-in. The data in Fig. 3 was obtained from averaging the 2PF endogenous response of 20-30

#255388 Received 10 Dec 2015; revised 2 Mar 2016; accepted 11 Mar 2016; published 24 Mar 2016

cells.

Decay rate calculation. The decay rate for each peak intensity, plotted in Fig. 3(b), was obtained by fitting the intensity from every pixel in the illuminated region of the image with an exponential function. The result was a spatially resolved map of the decay rates. We then calculated a probability distribution of the decay rates from which the overall decay rate for the measurement was obtained. In the probability distribution we only considered the values from locations in the image corresponding to a cell (i.e. the empty portions of the coverslip were not considered).

Acknowledgments

The authors would like to thank Aleksandra Radenovic and Alex de Beer for fruitful discussions, and Lely Feletti and Filip Ilievski for technical support. This work was supported by the Julia Jacobi Foundation, the Swiss National Foundation (grant number 200021-146884), and the European Commission, Research Executive Agency Marie Curie Actions 'FINON' (ITN-2013-607842).

#255388 Received 10 Dec 2015; revised 2 Mar 2016; accepted 11 Mar 2016; published 24 Mar 2016